Entropically-Driven Co-assembly of L-Histidine and L-Phenylalanine to Form Supramolecular Materials

*Om Shanker Tiwari[a], Ruth Aizen[a], Linda J. W. Shimon[b], Noam Tal[c], and Ehud Gazit[a,d,e]**

[a] The Shmunis School of Biomedicine and Cancer Research, The George S. Wise Faculty of Life Sciences, Tel Aviv University, Ramat Aviv, Tel Aviv 6997801, Israel.

[b] Department of Chemical Research Support, Weizmann Institute of Science, Rehovot, 7610001 Israel.

[c] School of Chemistry, Raymond and Beverly Sackler Faculty of Exact Sciences, Tel Aviv University, Ramat Aviv, Tel Aviv 6997801, Israel.

[d] Department of Materials Science and Engineering, The Iby and Aladar Fleischman Faculty of Engineering, Tel Aviv University, Ramat Aviv, Tel Aviv 6997801, Israel.

[e] Sagol School of Neuroscience, Tel Aviv University, Ramat Aviv, Tel Aviv 6997801, Israel.

AUTHOR INFORMATION.

*Corresponding Author

Address: The Shmunis School of Biomedicine and Cancer Research, The George S. Wise Faculty of Life Sciences, Tel Aviv University, Ramat Aviv, Tel Aviv 6997801, Israel.

Email: ehudga@tauex.tau.ac.il (Prof. Ehud Gazit)

ABSTRACT: Molecular self- and co-assembly allow the formation of diverse and well-defined supramolecular structures with notable physical properties. Among the associating molecules, amino acids are remarkably attractive due to their inherent biocompatibility and simplicity. The biologically-active enantiomer of L-Histidine (L-His) plays structural and functional roles in proteins but does not self-assemble to form discrete nanostructures. In order to expand the structural space to include L-His-containing materials, we explored the co-assembly of L-His with all aromatic amino acids, including Phenylalanine (Phe), Tyrosine (Tyr), and Tryptophan (Trp), all in both enantiomeric forms. In contrast to pristine L-His, the combination of this building block with all aromatic amino acids resulted in distinct morphologies including fibers, rods and flake-like structures. Electrospray ionization mass spectrometry (ESI-MS) indicated the formation of supramolecular co-assemblies in all six combinations, but time-of-flight secondary-ion mass spectrometry (ToF-SIMS) indicated the best seamless co-assembly occurs between L-His and L-Phe while in the other cases, different degrees of phase separation could be observed. Indeed, isothermal titration calorimetry (ITC) suggested the highest affinity between L-His and L-Phe where the formation of co-assembled structures was driven by entropy. In accordance, among all the combinations, co-assembly of L-His and L-Phe produced single crystals. The structure revealed the formation of a 3D network with nano-cavities stabilized by hydrogen bonding between -N (L-His) and -NH (L-Phe). Taken together, using the co-assembly approach we expanded the field of amino acid nano-materials and showed for the first time the ability to obtain discrete supramolecular nanostructures containing L-His based on its specific interactions with L-Phe.

KEYWORDS: Co-assembly, co-crystals, chirality, aromatic amino acids, supramolecular materials.

1. INTRODUCTION

Molecular self-assembly of amino acids allows the formation of various well-defined supramolecular structures with remarkable optical, mechanical, piezoelectric, and biological properties.[1-16] Amino acids are especially attractive building blocks for nanotechnological applications due to their chemical simplicity and inherent biocompatibility. Furthermore, increasing the chemical space by a co-assembly approach provides various supramolecular structures with improved physical, mechanical and electromechanical properties.[17-21] Natural aromatic amino acid building blocks, such as L-Phe, L-Tyr, and L-Trp, self-assemble by non-covalent interactions, including hydrogen bonding, aromatic interactions, and van der Waals interactions, to form amyloid-like well-ordered supramolecular assemblies.[1-9,22,23] Metal complexes of aromatic amino acids, such as L-Phe with Cu^{2+} and Zn^{2+} ions, can act as biocatalysts exhibiting high catalytic properties which can be useful in biotechnological, environmental protection, and industrial applications.[24,25] Crystal of Cu^{2+}-coordinated L-Phe and D-Phe showed significant magnetic properties that can be used in bioelectronics, spintronics and various technological applications.[26,27] Furthermore, amino acids are minimalistic building blocks that allow the design and improvement of the physicochemical properties of pristine supramolecular structures.[17,18,28-30] The co-assembly of aromatic amino acids and bipyridines in polar organic solvents exhibited 1D crystalline microarchitectures and this well-defined lamellar packing structure could act as a template to accommodate transition metal ions, allowing for the coordinated polymer growth of metal-bipyridine complexes.[31] Furthermore, the co-assembly of L-Phe and bipyridines resulted in smart high-quality hydrogel materials with light irradiation-triggered luminescence.[32] Co-assembly of aromatic amino acids enantiomers such as L/D-Phe and L/D-Trp exhibited flake-like supramolecular structures of high rigidity.[18]

Due to the heterocyclic imidazole ring in its side chain, L-His participates in enzyme-catalyzed reactions thereby playing a key role in various biological processes, including protein synthesis, metal ion coordination, proton buffering, reactive oxygen and nitrogen species removal.[33] The L-His imidazole ring can mediate an intermolecular interaction between phenyl and indole moieties in the side chains of L-Phe and L-His, respectively. This interaction can further stabilize the structures of various peptides and proteins through hydrogen bonding, NH-π, and π electrons interactions, which play an important role in biology and organic chemistry.[34-42] Furthermore, an L-His rich peptide was shown to form periodic arrays which can efficiently catalyze H_2O_2 reduction reactions through the formation of reactive ternary complex intermediates.[43,44] In a previous report, L-His was shown to display fluorescence properties in the powder form but not in the dissolved and self-assembled form which further suggests that L-His does not self-assemble into an ordered supramolecular nano-material using standard procedures.[45]

Herein, we investigated the self- and co-assembly of L-His with all the aromatic amino acid combinations namely L-His + L/D-Phe, L-His + L/D-Tyr, and L-His + L/D-Trp using X-ray diffraction, spectroscopy, spectrometry, microscopy, and thermodynamic analysis. Supramolecular structures of all the combinations were confirmed using high-resolution scanning electron microscopy (HRSEM), atomic force microscopy (AFM), optical microscopy, and high-resolution transmission electron microscopic (HRTEM) imaging techniques. Furthermore, co-assembly was corroborated by ToF-SIMS experiments followed by ESI-MS analysis. ITC experiments were performed to study the binding interaction and the thermodynamic parameter such as change in entropy (ΔS), change in enthalpy (ΔH), and change in Gibb's free energy (ΔG) of L-His with all the aromatic amino acid combinations. Moreover, single crystal X-ray diffraction (SCXRD) followed by powder X-ray diffraction (PXRD) experiments were performed to obtain

the crystal structure of the co-assembly of L-His with all the aromatic amino acids combinations. A thermogravimetric analysis (TGA) experiment was performed to confirm the thermal stability of the co-crystal of L-His with L-Phe. Finally, UV-Vis and circular dichroism (CD) measurements were performed to study the effect of π-π stacking interaction and the conformational changes due to the co-assembly of L-His with all the aromatic amino acid combinations. Our studies revealed that among all the aromatic amino acids, L-His forms the best seamless co-assembly with L-Phe. Additionally, only L-His exhibited the co-crystal with L-Phe and showed a strong interaction in fibrillar supramolecular assemblies, whereas other aromatic amino acids such as D-Phe, L/D-Tyr, and L/D-Trp displayed a weak affinity for L-His. The findings suggest an entropically-driven co-assembly approach for minimalistic building blocks such as amino acids, which can exhibit a variety of supramolecular structures for future nanotechnological applications.

2. RESULTS AND DISCUSSION

Here, we have investigated the self- and co-assembly of L-His with all aromatic amino acids, namely L/D-Phe, L/D-Tyr and L/D-Trp (Figure 1). L-His crystallized in water with the formation of sheet-like crystals. PXRD patterns (Figure S1a) confirmed the high crystalline properties of L-His. When studying the UV-Vis, L-His showed a strong UV band at 260 nm in the UV-Vis spectra (Figure S1b) and also a strong positive band at 234 nm in the CD spectra (Figure S1c) which are the characteristic peaks of L-His. The formation of a sheet-like morphological structure was confirmed using SEM (Figure 1Sd) and AFM (Figure 1Se). Next, we examined the combination of L-His with L/D-Phe, L/D-Tyr and L/D-Trp to obtain the diverse supramolecular structures. The assembled samples of different combinations were drop casted on a silicon wafer and the resulting morphology was examined by HRSEM. The assembly of L-His with L/D-Phe exhibited a fibrillar-like morphology (Figure 2a and 2b), L-His with L/D-Tyr produced rod-like structures (Figure 2c

and 2d) and L-His with L/D-Trp resulted in flake-like supramolecular structures (Figure 2e and 2f), as also supported by optical microscopy analysis (Figure S2).

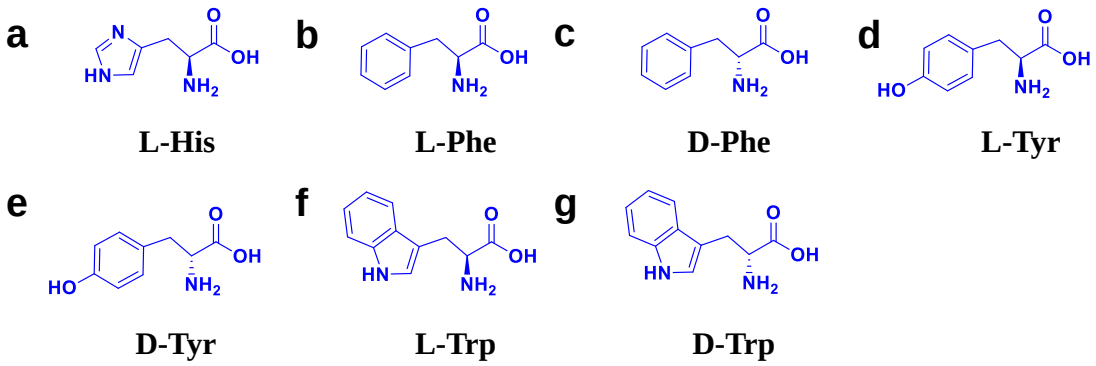

Figure 1. Chemical structures of aromatic amino acids. (a) L-His, (b) L-Phe, (c) D-Phe, (d) L-Tyr, (e) D-Tyr, (f) L-Trp, and (g) D-Trp.

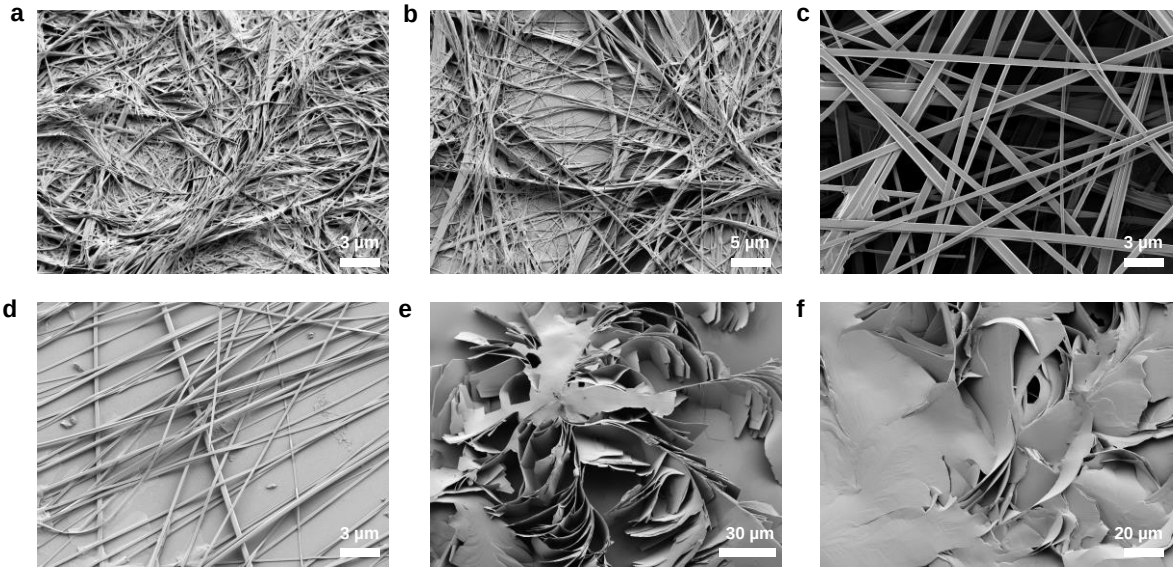

Figure 2. HRSEM images of (a) L-His + L-Phe (1:1), (b) L-His + D-Phe (1:1), (c) L-His + L-Tyr (1:1), (d) L-His + D-Tyr (1:1), (e) L-His + L-Trp (1:1), and (f) L-His + D-Trp (1:1) in water.

Previous reports suggest that the solvent plays an important role in the assembly process and specifically, dissolving in a 50% ethanol/water solution followed by lyophilization in 1,1,1,3,3,3-hexafluoro-2-propanol (HFIP) produced well-defined supramolecular structures, where HFIP was used to avoid the aggregation.[46,47] In order to further confirm the supramolecular structures obtained from the assembly of L-His with all the aromatic amino acid combinations, we first lyophilized all the amino acids at the concentration of 1 mg/mL in HFIP, and then diluted with 50% ethanol/water solution. We then mixed a 1:1 ratio of L-His with all other aromatic amino acids. HRSEM imaging showed that the assembly of L-His with all the aromatic amino acid combinations in a 50% EtOH/H_2O solution followed by lyophilization in HFIP exhibited similar results to the assembly in water (Figure 2 and Figure S3).

To further confirm the co-assembly process between L-His and all the aromatic amino acid combinations, ToF-SIMS experiments were performed. In a previous report, co-assembly of two different dipeptide building blocks, diphenylalanine (Phe-Phe) and *tert*-butyloxycarbonyl diphenylalanine (Boc-Phe-Phe), exhibited nanotubular supramolecular structures in solution and their monomeric presence was confirmed by ToF-SIMS.[48] Furthermore, the co-assembly of Phe-Phe and (((9H-fluoren-9-yl)methoxy)carbonyl)diphenylalanine (Fmoc-Phe-Phe) exhibited the formation of branched crystalline aggregates inside the supramolecular gel, comprised of both monomers was confirmed by ToF-SIMS.[21] It was further demonstrated that the co-assembly of two amino acids in a surface could be prepared by the vapor deposition technique of a solid amino acid mixture, as confirmed by ToF-SIMS.[19] The ToF-SIMS experiments can also be used for imaging within a phase-separated lipid membrane and measuring the amount of lipid present in specific areas of the bilayer.[49] For instance, ToF-SIMS investigations revealed that the formation of two distinct layers in the mixture of L-Phe with Gly and L-Phe with L-Ala could not

promote co-assembly and instead exhibited the self-sorted assemblies.[19] In our study, we first performed high-resolution mass spectroscopy in positive ion mode of self-assembly of all tested amino acids and then the co-assembly of L-His with all the aromatic amino acid combinations. High-resolution mass spectra from ToF-SIMS of L-His showed the peaks at *m*/*z* = 110, and 156, with the later corresponding to L-His and the former to a fragment of L-His (Figure S4a). A peak at 166 was observed for L-Phe (Figure S4b). Next, we analyzed the ToF-SIMS of the co-assembly of L-His and L-Phe (Figure 3 and Figure S4c). First, we performed the high-resolution mass spectra in positive ion mode which showed peaks at *m*/*z* = 156 and 166 corresponding to L-His and L-Phe, respectively (Figure 3a and Figure S4c), confirming the presence of both amino acids. HRSEM (Figure 3b) and ToF-SIMS ion images (Figure 3c-e) confirmed the presence of a fibrillar morphology in the co-assembly of L-His with L-Phe. To observe their location over a precise area chemical ion mapping was applied by selecting specific ions from the mass spectra (156 for L-His and 166 for L-Phe), clearly showing an overlap between the two ions in the fibrillar structures indicating the co-assembly of the two amino acids (Figure 3c-e).

ToF-SIMS experiments were further performed to examine the co-assembly of L-His with D-Phe, L/D-Tyr and L/D-Trp. High resolution mass spectra in positive ion mode of the assembly of L-His and D-Phe showed peaks at *m*/*z* = 156 and 166 corresponding to L-His and D-Phe, respectively, suggesting the presence of both the amino acids in the fibrillar supramolecular structures (Figure S5a). HRSEM imaging (Figure S5b) confirmed the presence of the fibrillar morphology. Chemical ion imaging of the ions corresponding to mass 156 (L-His) and 166 (D-Phe) showed a fibrillar supramolecular structure (Figure S5c and S5d). Yet, no significant overlap between the two ions was observed (Figure S5e), indicating that this amino acids pair could not form a co-assembly but rather self-sorted into fibrillar assemblies.

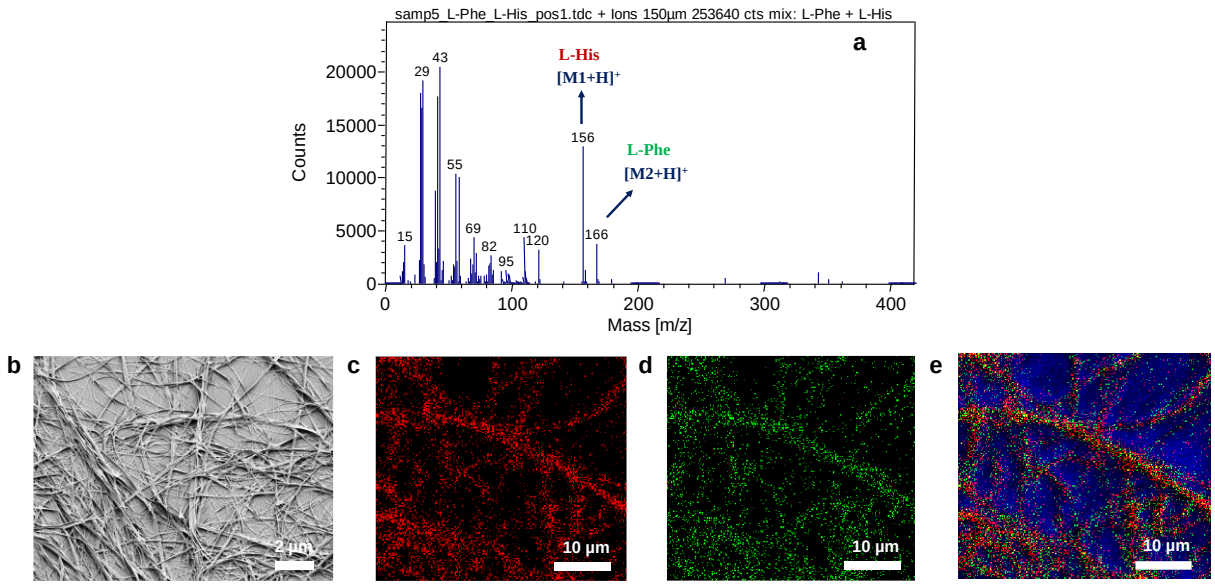

Figure 3. (a) High resolution mass spectra obtained from ToF-SIMS experiments using samples prepared by L-His and L-Phe mixture in water, showing the peaks at 156 (M1) and at 166 (M2) corresponding to L-His and L-Phe, respectively. (b) HRSEM image of co-assembly of L-His and L-Phe. (c-e) ToF-SIMS ion images of co-assembly of L-His + L-Phe. (c) L-His labelled in red color. (d) L-Phe labelled in green color. (e) A merged image of L-His and L-Phe.

Similarly, high resolution mass spectra in positive ion mode of the assembly of L-His with L/D-Tyr showed peaks at *m*/*z* = 156 and 182 corresponding to L-His and L-Tyr (Figure S6a) or L-His and D-Tyr (Figure S7a), respectively. HRSEM imaging (Figure S6b and S7b) confirmed the presence of rod-like supramolecular structures in the assembly of L-His with L/D-Tyr. Chemical ion imaging of the ions corresponding to mass 156 (L-His) and 182 (L/D-Tyr) showed a rod-like supramolecular structure (Figure S6c, S6d S7c, S7d), yet no significant overlap between the two ions was observed (Figure S6e and S7e). Thus, these amino acid pairs could not form a co-assembly but rather self-sorted into rod-like assemblies.

Finally, high resolution mass spectra in positive ion mode of the assembly of L-His with L/D-Trp showed peaks at *m/z* = 156 and 205 corresponding to L-His and L-Trp (Figure S8a), or L-His and D-Trp (Figure S9a), respectively. HRSEM images (Figure S8b and S9b) confirmed the presence of flake-like supramolecular structures in the assembly of L-His with L/D-Trp. Chemical ion imaging of the ions corresponding to mass 156 (L-His) and 205 (L/D-Trp) showed a flake-like supramolecular structure (Figure S8c, S9c, S8d and S9d). Furthermore, imaging of L-His (Figure S8c and S9c) and L/D-Trp (Figure S8d and S9d) showed no overlap in the merged ion image (Figure S8e and S9e) indicating that these amino acid pairs also could not form a co-assembly but rather self-sorted into flake-like supramolecular structures. Thus, from the ToF-SIMS experiments, it is clear that co-assembly took place only in the case of L-His + L-Phe which produced fibrillar supramolecular structures (Figure 3) whereas the other combinations could not form a co-assembly (Figure S5e, S6e, S7e, S8e, and S9e). Mass spectrometry has recently emerged as an important technique to understand the interaction between amino acids which exhibit various supramolecular structures and to detect the mass of amino acid complexes.[19] To further confirm the stability of the supramolecular structures due to the interaction of L-His with all aromatic amino acids, we performed an ESI-MS analysis of all the combinations. For the mixture of L-His and L-Phe, the *m/z* peaks at 154.2 and 164.2 in negative ion mode corresponding to L-His and L-Phe, respectively, were observed, as well as a signal for the L-His + L-Phe complex at 319.5. This also further suggested the formation of a co-assembled structure between L-His and L-Phe (Figure S10). Similarly, the signals of other complexes were also observed along with their individual peaks (Figure S11-S15). Thus, the ESI mass spectra clearly showed that the combined exact calculated masses of the assemblies of L-His with all the aromatic combinations match the observed mass (Figure S10-S15). Mass spectra further suggest the stability of different

supramolecular structures obtained from the assembly of L-His with all the aromatic amino acids combinations. Moreover, the ESI-MS analysis together with the ToF-SIMS experiments confirm the co-assembly of L-His with L-Phe which produces fibrillar supramolecular structures.

Furthermore, As previously reported, the interactions between amino acids, peptides and protein, and specifically entropy-driven interactions, were confirmed through thermodynamic parameter calculations using an ITC analysis.[19,50-52] To further study the interactions and thermodynamic parameters, ITC experiments were performed for L-His with all the aromatic amino acids. A freshly prepared solution of L-His (80 mM) was titrated into a cell containing each of the other aromatic amino acids (4 mM). The results of the titration profile and the calculated thermodynamic parameters are presented (Figure 4 and Figure S16-S20; Table 1). The calculated dissociation constants (K_D in M) confirmed that L-His strongly interacted with L-Phe (2.0×10^{-4}), while L-His with all the other aromatic amino acids combinations, namely L-His + D-Phe (8.85×10^{-4}), L-His + L-Tyr (7.86×10^{-4}), L-His + D-Tyr (8.64×10^{-4}), L-His + L-Trp (8.94×10^{-4}), and L-His + D-Trp (8.49×10^{-4}), resulted in almost four times higher K_D values. Interestingly, the titrations of L-His with all the aromatic amino acids resulted in exothermal peaks (Figure 4a and Figure S16a, S17a, S18a, S19a, S20a). Enthalpy change (ΔH) decreases, forming a sigmoidal curve after increasing the molar fraction of L-His with all the aromatic amino acids (Figure 4b and Figure S16b, S17b, S18b, S19b, S20b), and further suggesting that the process is driven by entropy. Based on the ITC data presented in Table 1, it is clear that $T\Delta S > \Delta H$ which resulted in $\Delta G < 0$ in all cases, suggesting that the interaction of L-His with all the aromatic amino acid combination was a spontaneous process. Also, the change in entropy ($-T\Delta S = -21.30$ (kJ/mol)) is the highest for the co-assembly of L-His and L-Phe confirming that L-His has the highest affinity to co-assemble with L-Phe.

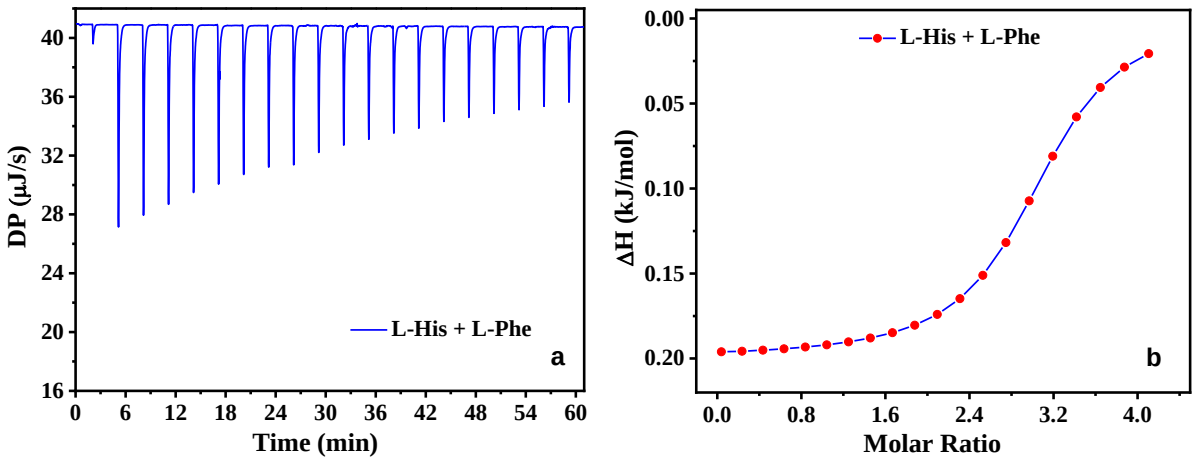

Figure 4. (a) Heat pattern during L-His + L-Phe amino acids binding. (b) Curves showing the enthalpy changes upon increasing the L-His molar fraction in 1x PBS buffer at pH = 7.22.

Table 1. Thermodynamic analysis of binding of L-His with all aromatic amino acids by ITC measurements in 1x PBS buffer at pH = 7.22.

Sr. No.	**Combination of amino acids**	**K_D (x 10^{-4} M)**	**ΔH (kJ/mol)**	**ΔG (kJ/mol)**	**-TΔS (kJ/mol)**
1.	L-His : L-Phe	2.00 ± 0.570	0.199 ± 0.005	-21.10	-21.30
2.	L-His : D-Phe	8.85 ± 0.719	0.414 ± 0.005	-17.40	-17.90
3.	L-His : L-Tyr	7.86 ± 0.775	0.379 ± 0.006	-17.70	-18.10
4.	L-His : D-Tyr	8.64 ± 0.796	0.402 ± 0.006	-17.50	-17.90

5.	L-His : L-Trp	8.94 ± 0.784	0.424 ± 0.006	-17.40	-17.80
6.	L-His : D-Trp	8.49 ± 0.693	0.410 ± 0.005	-17.50	-18.00

Additionally, to obtain more insight into the assembly of L-His with aromatic amino acids, we tried the co-crystallization of all the combinations under different conditions, such as solvent, concentration, temperature, etc. Among all the combinations, we were able to obtain the single crystal structure of L-His + L-Phe co-crystal in water only. A good quality plate-like colorless crystal of L-His + L-Phe, suitable for solid-state SCXRD analysis was obtained by dissolving both amino acids in water at different concentration followed by slow evaporation. Nevertheless, all other combinations showed patterns that were different from the individual amino acids in the PXRD which supported the co-crystalline behavior but were not suitable for SCXRD (Figure S21). Optical microscopy images of the assembly of L-His + D-Phe, L-His + L-Tyr and L-His + D-Tyr exhibited rod-like colorless crystals (Figure S22a-c) while L-His + L-Trp and L-His + D-Trp produced sheet-like colorless crystals (Figure S22d and S22e). The crystal structure of L-His + L-Phe co-crystal revealed that it crystalized in the orthorhombic crystal system with the space group $P2_12_12_1$ (Figure 5a, Figure S23, S24a and Table S1). ORTEP diagram and unit cell representation of the crystal structure also confirmed that the co-crystal contained both monomers (Figure S23) with two molecules of L-His and two molecules of L-Phe per asymmetric unit cell (Figure S23b) in an orthorhombic arrangement. This co-crystal formation took place due to the hydrogen bonding between -N (L-His) and -NH (L-Phe) with a bond distance of 2.883 Å (N12-----N17) (Figure 5a, Figure S24a and Table S2). The chemical representation of the hydrogen bond in the co-crystal of

L-His + L-Phe (Figure 5b) was confirmed from the single crystal structure (Figure 5 and Figure S24). Further, packing of the crystal structure confirmed that the co-crystal of L-His + L-Phe crystalized into a 3D network-like structure with different sizes of the nano-cavities due to the hydrogen bonding between both amino acids (Figure 5c, 5d and Figure S24b, S24c). The bond distances between N12-----N17, N12-----O21, N15-----O10, N17-----O11, N23-----O11were 2.883, 5.316, 2.873, 4.321, and 6.549 Å, respectively (Figure 5c and Table S2). The 3D crystal packing data also indicated the presence of a repeating unit in the packing of the crystal structure (Figure S24c). The aromatic amino acids were also re-crystalized in water followed by heating at 90 ^{o}C, lyophilized and their recorded PXRD data were matched with the PXRD references (Table S3). The crystalline properties of the co-crystal of L-His and L-Phe were further confirmed by using the PXRD pattern (Figure 6a) which showed the presence of different patterns in the co-crystal compared to the individual L-His and L-Phe. Since the L-His + L-Phe co-crystals were solid, we performed a TGA measurement to further examine their thermal stability and found is the co-crystal to be stable up to more than 220 ^{o}C which is significant in the case of such small organic building blocks (Figure S25).

To further study the effect of aromatic stacking interactions and conformations of the co-assembly of L-His with all the aromatic amino acids combinations, we performed UV-Vis (Figure 6b and Figure S26) and CD spectroscopy experiments (Figure 6c and Figure S27). UV-Vis spectra of the co-assembly of L-His + L-Phe represented the combined effect of L-His with L-Phe, suggesting no shift in the peak following co-assembly (Figure 6b). UV-Vis spectroscopy of all the other aromatic amino acid combinations with L-His showed that there was no change in the UV-Vis spectra of assembly of L-His with L/D-Phe and L-His with L/D-Tyr (Figure S26a-c). A small

shift was observed in the UV-Vis spectra of L-His + L-Trp and L-His + D-Trp which may be due to the π-π stacking interactions between L-His and L/D-Trp (Figure S26d and S26e).

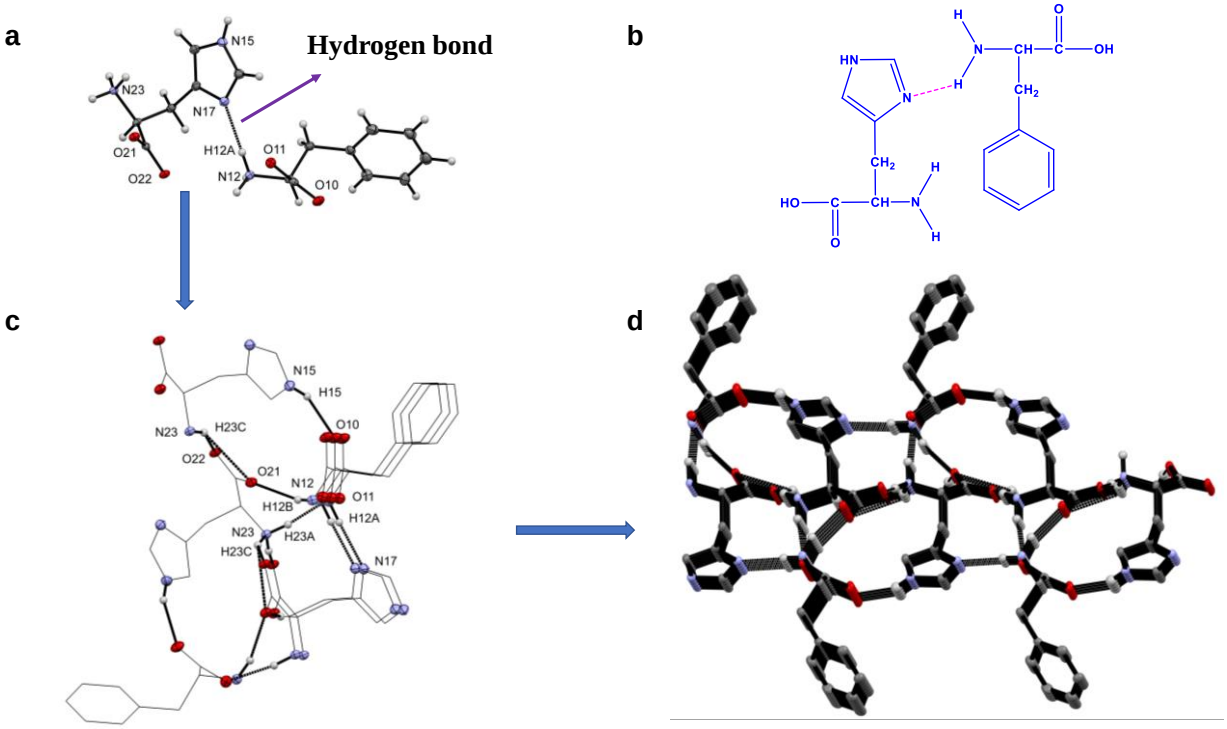

Figure 5. (a) Single crystal structure of a co-crystal of L-His + L-Phe. (b) Chemical structure of the co-assembly of L-His + L-Phe mediated through hydrogen bonding. (c) Hydrogen bonding interactions in the co-crystal. (d) A 3D network-like structure showing different sizes of cavities.

To further study the conformational properties, we performed CD spectra and found that L-His, L-Phe and the co-assembly of L-His + L-Phe exhibited positive bands (Figure 6c). The peak of co-assembled L-His + L-Phe was intermediate between the peak of L-His and L-Phe which may be due to their combined conformational effect (Figure 6c). This also further supports the co-assembly between L-His and L-Phe. Furthermore, the fibrillar supramolecular structure of the co-assembly of L-His + L-Phe were confirmed by HRSEM (Figure S28a), HRTEM (Figure 6d and Figure S28b) and optical microscopy images (Figure 6e and Figure S28c). Optical microscopy

image confirms the plate-like colorless crystal of the co-crystal of L-His and L-Phe (Figure 6f and S28d). The fibrillar supramolecular morphology of the co-assembly of L-His + L-Phe was further confirmed by AFM imaging (Figure S29a and S29b). Height profile obtained from the AFM images suggested the height of fibers to be in the nanometer range (Figure S29c). Finally, time-dependent study was performed to check the change in the morphology of the fibrillar structures showing that the fibrillar supramolecular structures obtained from the co-assembly of L-His and L-Phe were stable even after 10 days (Figure S30).

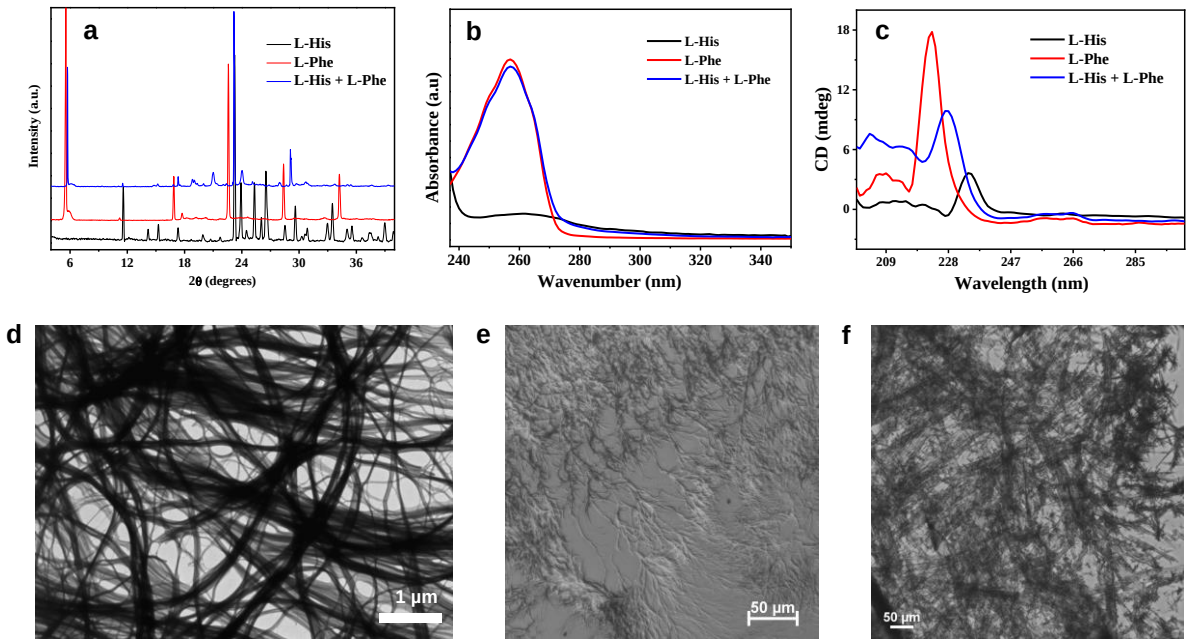

Figure 6. (a) PXRD pattern of co-crystal of L-His + L-Phe. (b-e) Analysis of the co-assembly of L-His + L-Phe in water. (b) UV-Vis spectra. (c) CD spectra. (d) HRTEM image. (e) Optical microscopy image. (f) Optical microscopy image of co-crystal of L-His + L-Phe in water.

Furthermore, D-Phe showed a negative band in the CD spectra and co-assembly of L-His + D-Phe produced a slight negative band which may be due to the cancellation of the L-His and D-Phe bands in the CD spectrum and higher CD band intensity of D-Phe compared to L-His, resulting in

the negative band of the co-assembly (Figure S27a). Furthermore, CD spectra of L-Tyr and D-Tyr showed a positive and negative band, respectively, and their combinations with L-His exhibited the combined effect of L-His + L-Tyr (Figure S27b) and L-His + D-Tyr (Figure S27c). Finally, L-Trp and D-Trp exhibited positive (Figure S27d) and negative band (Figure S27e), respectively. The combination of L-His with L-Trp produced a positive CD band due to the positive bands of both monomers (Figure S27d) whereas the co-assembly of L-His with D-Trp exhibited a negative band due to cancellation of L-His (positive band) and D-Trp (negative band). The resultant CD spectrum of the co-assembly of L-His with D-Trp was a negative band due to the low intensity of the positive band (L-His) and high intensity of the negative band (D-Trp) (Figure S27e) which further suggests that the CD spectra of L-His with all the aromatic amino acid combinations are the result of the CD spectra of the two amino acids individually (Figure S27).

3. CONCLUSIONS

The self-assembly of L-His and its co-assembly with all the aromatic amino acids, namely L/D-Phe, L/D-Tyr and L/D-Trp, were investigated. L-His exhibited sheet-like morphology in water which was confirmed using HRSEM and AFM whereas the co-assembly of L-His with all the aromatic amino acids produced different supramolecular structures such as fibrillar, rods and flake-like morphology. While ToF-SIMS analysis further confirmed the co-assembly of L-His with L-Phe and there is no co-assembly in the other combinations. In contrast, ESI-MS findings show that all six combinations formed supramolecular co-assemblies. A possible explanation for the disparity between the two results is that, with the exception of L-His + L-Phe, all other combinations form co-assemblies in solutions but not in the solid state. ESI-MS experiments also supported the stability of all the supramolecular structures. Moreover, ITC results suggested the presence of strong binding interactions between L-His and all the aromatic amino acids. The lowest

K_D value (2.0 x 10^{-4} M) was found for the L-His + L-Phe which also further confirms the presence of strong interactions between L-His and L-Phe. Only the L-His + L-Phe amino acid combination resulted in the formation of a co-crystal. The co-crystalline properties of L-His + L-Phe were confirmed using SCXRD showing an orthorhombic, non-centrosymmetric crystal system, suggesting potentially-applicable piezoelectric properties. The single crystal structure of the co-assembly between L-His and L-Phe revealed the formation of a 3D network-like structure with different sizes of nano-cavities due to the hydrogen bonding between both amino acids. TGA data showed the thermal stability of the co-crystal up to >220 ^{o}C which is significant in the case of single amino acids. Furthermore, the highest change in entropy was detected for the co-assembly of L-His and L-Phe which also confirms that L-His has the highest binding affinity to co-assemble with L-Phe. The fibrillar supramolecular structure obtained from the co-assembly of L-His with L-Phe was confirmed using HRSEM, optical microscope, HRTEM and AFM imaging. The formation of plate-like colorless crystals by L-His + L-Phe was confirmed by optical microscopy. Time-dependent study using SEM imaging did not detect any new morphological structures which further suggests the stability of the supramolecular structures. UV-Vis and CD spectra supported the combined effect of L-His with all the aromatic amino acids. Further, it was also confirmed that there is no change in the supramolecular structures due to the chirality as the co-assembly of L-His with each pair of amino acid enantiomers resulted in a similar morphology, regardless of the chirality. This work lays the foundations to study the self- and co-assemblies of simple and minimalistic building blocks such as amino acids to design various new supramolecular structures for biological, material science and nanotechnological applications.

4. EXPERIMENTAL SECTION

4.1. Materials and methods: All the amino acids were purchased from Sigma Aldrich (purity > 98%). Water was processed using a Millipore purification system (Biological Industries, Beit Haemeck, Israel) with a minimum resistivity of 18.2 MΩ cm.

4.2. Spectroscopic data

Compound 1 [L-His + L-Phe, (M)]: ESI Mass spectra (ESI^-), m/z calculated for $(M-H)^-$ $C_{15}H_{19}N_4O_4$: 319.2, found: 319.5.

Compound 2 [L-His + D-Phe, (M)]: ESI Mass spectra (ESI^-), m/z calculated for $(M-H)^-$ $C_{15}H_{19}N_4O_4$: 319.2, found: 319.3.

Compound 3 [L-His + L-Tyr, (M)]: ESI Mass spectra (ESI^-), m/z calculated for $(M-H)^-$ $C_{15}H_{19}N_4O_5$: 335.1, found: 335.4.

Compound 4 [L-His + D-Tyr, (M)]: ESI Mass spectra (ESI^-), m/z calculated for $(M-H)^-$ $C_{15}H_{19}N_4O_5$: 335.1, found: 335.4.

Compound 5 [L-His + L-Trp, (M)]: ESI Mass spectra (ESI^-), m/z calculated for $(M-H)^-$ $C_{17}H_{20}N_5O_4$: 358.2, found: 358.4.

Compound 6 [L-His + D-Trp, (M)]: ESI Mass spectra (ESI^-), m/z calculated for $(M-H)^-$ $C_{17}H_{20}N_5O_4$: 358.2, found: 358.3.

4.3. Powder X-Ray diffraction (PXRD): All the aromatic amino acids and their co-crystals with L-His were crystallized in ultrapure water (Biological Industries, Beit Haemeck, Israel), after which the sample was filtered and completely dried under vacuum before performing the PXRD experiments. The self- or co-assembled aromatic amino acids crystal powder samples were

deposited on a quartz zero-background sample holder. PXRD pattern was collected using a Bruker D8 Discover diffractometer (Bruker, Germany) equipped with Goebels mirrors to parallelize the beam and LYNXEYE-XE linear detector. Data collection was performed at room temperature with a scan range 2θ of 2-40°.

4.4. UV-Vis spectroscopy: UV-Vis measurements were performed using a Cary Series UV-Vis spectrophotometer (model Cary 100 UV-Vis; Agilent Technologies). A quartz cuvette with an optical path length of 1 mm was used for all the measurements.

4.5. Circular dichroism (CD) spectroscopy: CD spectrometry study was carried out on a Chirascan CD spectropolarimeter using cylindrical, jacketed quartz cell (path length of 10 mm) connected to Julabo-UC25 water circulator. The wavelengths range was 190 nm to 300 nm. For reproducible data, each set of spectra were measured using at least three individually prepared solutions. CD spectra were recorded using a spectral bandwidth of 1.0 nm at 25 °C with a time constant of 1 s and a step resolution of 1 nm. All spectra were recorded in water and typically averaged over 3-5 scans. A quartz cell with a path length of 1 mm was used with solutions containing approximately 0.25 mL (1 mM). All the spectra were obtained following solvent background subtraction. Data processing and curve fitting were performed using Origin 8.0 software.

4.6. High-resolution scanning electron microscopy (HRSEM): Amino acid powders were dissolved in deionized water by heating at 90 °C at a concentration of 1 mg/mL, followed by vortex to obtain a clear, transparent solution. The mixture was then allowed to gradually cool down overnight leading to self- and co-assembly for all the amino acids. For co-assembly, the solution of L-His was mixed with each aromatic amino acid solution under heating condition at a 1:1 ratio

and allowed to cool down gradually. A 5 µL aliquot was allowed to dry on a silicon wafer at ambient conditions overnight and coated with Au. HRSEM images were collected using Zeiss Gemini 300 (Zeiss, Germany) with an operating voltage of 3 kV.

The co-assembly process was further monitored after lyophilization in HFIP, followed by dilution in 50% ethanol/water at 1 mg/mL. After deposition on silicon surface, samples were dried at room temperature and imaged.

4.7. Atomic force microscopy (AFM): Co-assembled L-His + L-Phe sample (5 µl, 1 mg / mL in water) was drop casted on freshly cleaved SiO_2/Si substrate, and air dried at room temperature. AFM images were recorded using AFM (JPK Instruments AG) performed with Nano Wizard 3 using 5 N/m spring constant tips and a resonance frequency of ~150 kHz in soft tapping mode. AFM analysis was conducted on different areas for each sample, and the height was measured using the Gwyddoin 2.56 software.

4.8. Optical microscopy: The co-assembled supramolecular structures and co-crystal were prepared in water, drop casted on a glass slide, and directly observed using a Nikon Eclipse Ti-E florescence microscope at bright field channels.

4.9. Time-of-flight secondary ion mass spectrometry (ToF-SIMS): The self- and co-assembled aromatic amino acids were deposited on silicon wafer and analyzed using a PHI Model 2100 TRIFT II ToF-SIMS instrument. The system used a pulsed primary ion beam to desorb and ionize species from the amino acids surface. The resulting secondary ions were accelerated into a mass spectrometer, where the mass was analyzed by measuring the time-of-flight from the sample surface to the detector. Furthermore, an image was generated by rostering a finely focused beam across the self- and co-assembled sample surface. Due to the parallel detection properties of ToF-

SIMS, the entire mass spectrum was acquired from every pixel in the image. The ions related to m/z = 156, m/z = 166, m/z = 182, and m/z = 205 were used to identify and evaluate the ionic image of L-His^+, L/D-Phe^+, L/D-Tyr^+, and L/D-Trp^+, respectively. The high-resolution mass spectrum and the secondary ion images were then used to determine the composition and distribution of sample surface constituents.

4.10. Mass spectrometry: Co-assembly samples were prepared for mass spectrometry by dissolving the amino acids at a concentration of 1 mg/mL in deionized water by heating to 90 °C followed by gradual cooling. Mass spectrometry was recorded using an Acquity UPLC system coupled to a TQD XEVO triple quadrupole ESI source mass spectrometer system from Waters (Milford, MA, USA). Mass spectrometry was done by ESI, measuring both positive and negative ionization.

4.11. Isothermal titration calorimetry (ITC): Freshly prepared L-His (80 mM) was dissolved in 1x PBS. L/D-Phe, L/D-Tyr and L/D-Trp were diluted in 1x PBS to a working concentration of 4 mM. All the titration experiments were performed at 25 °C in 1x PBS buffer (pH 7.22). The instrument was equilibrated at 25 °C until the baseline was flat and stable. The stirring speed was maintained at 700 rpm during the titrations. The solutions were kept at 25 °C until measurement. A 350 μL sample of the L/D-Phe, L/D-Tyr and L/D-Trp solution was inserted into the Nano ITC low volume cell (Malvern MicroCal PEAQ-ITC), and the titrating syringe was filled with 50 μL L-His solution. The excess solution was removed from the cell before performing the experiments. The system was allowed to reach a stable temperature of 25 °C along 600 s and collected baseline sample for 120 s. Subsequently, L-His was titrated to the PBS as a control and subtracted from the final measurements. Titration was carried out in 2 μL aliquots and allowed to equilibrate for 180 s before the next drop, along 20 drops, at a total of 38.5 μL (first drop was half volume). The

resulting isotherm was analyzed using Malvern MicroCal PEAQ- ITC analysis software using an independent interaction model. The binding isotherm was fitted to a "one set of binding sites" model.

4.12. Crystal preparation and data collection: Crystals used for data collection were grown using the slow solvent evaporation method. The dry amino acids were first dissolved in Milli-Q water at the concentrations of 100 mg/mL and 40 mg/mL for L-His and L-Phe, respectively. Then, both samples are heated at 90 ^{o}C followed by vortex to dissolved them completely. Both completely-dissolved solutions were mixed at 90 ^{o}C and it was allowed to cool down gradually. Plate-like L-His + L-Phe co-crystal formation took place after few days by slow evaporation of the water solvent. For data collection, crystals were coated in Paratone oil (Hampton Research), mounted on a MiTeGen cryo-loop, and flash frozen in liquid nitrogen. Single crystal diffraction data were collected at 100 K on a Rigaku XtaLAB Synergy R rotating anode system with a HyPix-Arc 150 detector using CuKα radiation at λ = 1.54184 Å.

4.13. Processing and structural refinement of crystal data: The diffraction data were collected and processed was performed using the CrysAlisPro 1.171.41.111a of programs (RigakuOD 2021). The structures were solved by direct methods using SHELXT-2018 and refined by full-matrix least squares against F2 with SHELXL-2016. Atoms were refined independently and anisotropically, with the exception of hydrogen atoms, which were placed in calculated positions and refined in a riding mode. Crystal data collection and refinement parameters are shown in Supplementary Table S1, and the complete data can be found in the cif file as Supporting Information. The crystallographic data have been deposited in the CCDC with nos. 2193020 for L-His + L-Phe.

4.14. Thermal gravimetric analysis (TGA): TGA of the L-His + L-Phe co-crystal was performed using a TA Instruments (USA) module SDT 2950, at a temperature range between 40 and 800 °C with a heating rate of 10 °C min^{-1}, under a dry ultrahigh-purity argon atmosphere.

4.15. Transmission electron microscopy (TEM): The co-assembled L-His + L-Phe sample (5 µl, 1 mg / mL in water) was drop casted on a 400-mesh carbon-stabilized Formvar-coated Cu grid (Ted Pella, California, USA). The sample was allowed to bind the surface for 2 min and then the excess sample was removed using a lint free tissue, dried at room temperature and imaged. Sample morphology was visualized using a JEM-1400 TEM (JEOL, Tokyo, Japan) accelerating at 80 kV.

Accession Codes

CCDC 2193020 contain the supplementary crystallographic data of co-crystal of L-His + L-Phe for this paper. These data can be obtained free of charge via www.ccdc.cam.ac.uk/data_request/cif, or by emailing data_request@ccdc.cam.ac.uk, or by contacting The Cambridge Crystallographic Data Centre, 12 Union Road, Cambridge CB2 1EZ, UK; fax: +44 1223 336033.

ASSOCIATED CONTENT

Supporting Information: The Supporting Information is available online.

Figure S1-S30: PXRD, UV-Vis, CD, SEM, and AFM image of L-His; SEM images of all 7 amino acids; Optical microscope, HRSEM images, ToF-SIMS data, ESI-MS, and ITC data of all the 6 combinations; PXRD patterns and optical microscope images of all the 6 combined crystals; single crystal structure and TGA data of the co-crystal of L-His + L-Phe. UV-Vis and CD data of all the 6 combinations; HRSEM, optical microscope, HRTEM, AFM image of the fibers obtained from the co-assembly of L-His + L-Phe; Optical microscope image of the co-crystal of L-His + L-Phe;

Time dependent SEM images of the co-assembly of L-His + L-Phe. **Table S1-S3**: Crystallographic data collection and refinement statistics data for co-crystal of L-His + L-Phe; Bond distance for the co-crystal of L-His + L-Phe from single crystal structure; List of PXRD references (Powder Diffraction File) for the self-assembled and lyophilized samples (PDF).

Conflicts of interest

There are no conflicts of interest to declare.

ACKNOWLEDGMENT

We thank Dr. Sigal Rencus-Lazar for excellent editing of the text. O. S. T. thanks the Tel Aviv University for fellowship and financial support. E. G. thanks the Airforce research laboratories (AFRL) for support. This material is based on work supported by the Air Force Office of Scientific Research under award number FA8655-21-1-7004. Any opinions, findings, and conclusions or recommendations expressed in this material are those of the authors and do not necessarily reflect the views of the United States Air Force.

5. REFERENCES

(1) Chakraborty, P.; Gazit, E. Amino Acid Based Self-assembled Nanostructures: Complex Structures from Remarkably Simple Building Blocks. *ChemNanoMat* **2018**, *4*, 730-740.

(2) Ji, W.; Xue, B.; Arnon, Z. A.; Yuan, H.; Bera, S.; Li, Q.; Zaguri, D.; Reynolds, N. P.; Li, H.; Chen, Y.; Gilead, S.; Rencus-Lazar, S.; Li, J.; Yang, R.; Cao, Y.; Gazit, E. Rigid Tightly Packed Amino Acid Crystals as Functional Supramolecular Materials. *ACS Nano* **2019**, *13*, 14477-14485.

(3) Adler-Abramovich, L.; Vaks, L.; Carny, O.; Trudler, D.; Magno, A.; Caflisch, A.; Frenkel, D.; Gazit, E. Phenylalanine Assembly into Toxic Fibrils Suggests Amyloid Etiology in Phenylketonuria. *Nat. Chem. Biol*. **2012**, *8*, 701-706.

(4) Tomar, D.; Chaudhary, S.; Jena, K. C. Self-assembly of L-phenylalanine amino acid: electrostatic induced hindrance of fibril formation. *RSC Adv.* **2019**, *9*, 12596-12605.

(5) Ren, H.; Wu, L.; Tan, L.; Bao, Y.; Ma, Y.; Jin, Y.; Zou, Q. Self-assembly of amino acids toward functional biomaterials. *Beilstein J. Nanotechnol.* **2021**, *12*, 1140-1150.

(6) Shaham-Niv, S.; Rehak, P.; Vuković, L.; Adler-Abramovich, L.; Král, P.; Gazit, E. Formation of Apoptosis-Inducing Amyloid Fibrils by Tryptophan. *Isr. J. Chem.* **2017**, *57*, 729-737.

(7) Shaham-Niv, S.; Arnon, Z. A.; Sade, D.; Lichtenstein, A.; Shirshin, E. A.; Kolusheva, S.; Gazit, E. Intrinsic Fluorescence of Metabolite Amyloids Allows Label-Free Monitoring of Their Formation and Dynamics in Live Cells. *Angew. Chem. Int. Ed*. **2018**, *57*, 12444-12447.

(8) Singh, V.; Rai, R. K.; Arora, A.; Sinha, N.; Thakur, A. K. Therapeutic implication of L-phenylalanine aggregation mechanism and its modulation by D-phenylalanine in phenylketonuria. *Sci. Rep*. **2014**, *4*, 3875.

(9) De Luigi, A.; Mariani, A.; De Paola, M.; Re Depaolini, A.; Colombo, L.; Russo, L.; Rondelli, V.; Brocca, P.; Adler-Abramovich, L.; Gazit, E.; Del Favero, E.; Cantu, L.; Salmona, M. Doxycycline hinders phenylalanine fibril assemblies revealing a potential novel therapeutic approach in phenylketonuria. *Sci. Rep*. **2015**, *5*, 15902.

(10) Zaguri, D.; Shaham-Niv, S.; Chakraborty, P.; Arnon, Z.; Makam, P.; Bera, S.; Rencus-Lazar, S.; Stoddart, P. R.; Gazit, E.; Reynolds, N. P. Nanomechanical Properties and Phase Behavior of Phenylalanine Amyloid Ribbon Assemblies and Amorphous Self-Healing Hydrogels. *ACS Appl. Mater. Interfaces* **2020**, *12*, 21992-22001.

(11) Zaguri, D.; Kreiser, T.; Shaham-Niv, S.; Gazit, E. Antibodies towards Tyrosine Amyloid-Like Fibrils Allow Toxicity Modulation and Cellular Imaging of the Assemblies. *Molecules* **2018**, *23*, 1273.

(12) Tiwari, O. S.; Rencus-Lazar, S.; Gazit, E. Advances in Self-Assembly of Metabolite Nanostructures: Physiology, Pathology and Nanotechnology. *ChemNanoMat* **2022**, *8*, e202200055.

(13) Moazeni, M.; Karimzadeh, F.; Kermanpur, A. Investigation and regulation of self-assembled well-ordered nano/microstructures via an aromatic α-amino acid. *Soft Matter*, **2018**, *14*, 4996-5007.

(14) Shaham-Niv, S.; Adler-Abramovich, L.; Schnaider, L.; Gazit, E. Extension of the generic amyloid hypothesis to nonproteinaceous metabolite assemblies. *Sci. Adv.* **2015**, *1*, e1500137.

(15) Menard-Moyon, C.; Venkatesh, V.; Krishna, K. V.; Bonachera,́ F.; Verma, S.; Bianco, A. Self-Assembly of Tyrosine into Controlled Supramolecular Nanostructures. *Chem. Eur. J.* **2015**, *21*, 11681-11686.

(16) Guerin, S.; Tofail, S. A. M.; Thompson, D. Longitudinal Piezoelectricity in Orthorhombic Amino Acid Crystal Films. *Cryst. Growth Des*. **2018**, *18*, 9, 4844-4848.

(17) Ji, W.; Xue, B.; Bera, S.; Guerin, S.; Shimon, L. J.W.; Ma, Q.; Tofail, S. A. M.; Thompson, D.; Cao, Y.; Wang, W.; Gazit, E. Modulation of physical properties of organic cocrystals by amino acid chirality. *Materials Today*, **2021**, *42*, 29-40.

(18) Bera, S.; Xue, B.; Rehak, P.; Jacoby, G.; Ji, W.; Shimon, L. J. W.; Beck, R.; Král, P.; Cao, Y.; Gazit, E. Self-Assembly of Aromatic Amino Acid Enantiomers into Supramolecular Materials of High Rigidity. *ACS Nano* **2020**, *14*, 1694-1706.

(19) Bera, S.; Mondal, S.; Tang, Y.; Jacoby, G.; Arad, E.; Guterman, T.; Jelinek, R.; Beck, R.; Wei, G.; Gazit, E. Deciphering the Rules for Amino Acid Co-Assembly Based on Interlayer Distances. *ACS Nano* **2019**, *13*, 2, 1703-1712.

(20) Makam, P.; Gazit, E. Minimalistic peptide supramolecular co-assembly: expanding the conformational space for nanotechnology. *Chem. Soc. Rev*. **2018**, *47*, 3406-3420.

(21) Chakraborty, P.; Tang, Y.; Guterman, T.; Arnon, Z. A.; Yao, Y.; Wei, G.; Gazit, E. Co-Assembly between Fmoc Diphenylalanine and Diphenylalanine within a 3D Fibrous Viscous Network Confers Atypical Curvature and Branching. *Angew. Chem. Int. Ed.* **2020**, *59*, 23731-23739.

(22) Babar, D. G.; Sarkar, S. Self-assembled nanotubes from single fluorescent amino acid. *Appl. Nanosci*. **2017**, *7*, 101-107.

(23) Singh, P.; Brar, S. K.; Bajaj, M.; Narang, N.; Mithu, V. S.; Katare, O. P.; Wangoo, N.; Sharma, R. K. Self-assembly of aromatic α-amino acids into amyloid inspired nano/micro scaled architects. *Mater. Sci. Eng.* C **2017**, *72*, 590-600.

(24) Makam, P.; Yamijala, S. S. R. K. C.; Bhadram, V. S.; Shimon, L. J. W.; Wong, B. M.; Gazit, E. Single amino acid bionanozyme for environmental remediation. *Nat. Commun*. **2022**, *13*, 1505.

(25) Makam, P.; Yamijala, S. S. R. K. C.; Tao, K.; Shimon, L. J. W.; Eisenberg, D. S.; Sawaya, M. R.; Wong, B. M.; Gazit, E. Non-proteinaceous hydrolase comprised of a phenylalanine metallo-supramolecular amyloid-like structure. *Nat. Catal*. **2019**, *2*, 977-985.

(26) Mondal, A. K.; Brown, N.; Mishra, S.; Makam, P.; Wing, D.; Gilead, S.; Wiesenfeld, Y.; Leitus, G.; Shimon, L. J. W.; Carmieli, R.; Ehre, D.; Kamieniarz, G.; Fransson, J.; Hod, O.; Kronik, L.; Gazit, E.; Naaman, R. Long-Range Spin-Selective Transport in Chiral Metal–Organic Crystals with Temperature-Activated Magnetization. *ACS Nano* **2020**, *14*, 16624-16633.

(27) Goren, N.; Das, T. K.; Brown, N.; Gilead, S.; Yochelis, S.; Gazit, E.; Naaman, R.; Paltiel, Y. Metal Organic Spin Transistor. *Nano Lett*. **2021**, *21*, 8657-8663.

(28) Nugrahani, I.; Jessica, M. A. Amino Acids as the Potential Co-Former for Co-Crystal Development: A Review. *Molecules* **2021**, *26*, 3279.

(29) Ji, W.; Yuan, C.; Chakraborty, P.; Makam, P.; Bera, S.; Rencus-Lazar, S.; Li, J.; Yan, X.; Gazit, E. Coassembly-Induced Transformation of Dipeptide Amyloid-Like Structures into Stimuli-Responsive Supramolecular Materials. *ACS Nano* **2020**, *14*, 7181-7190.

(30) Ji, W.; Yuan, H.; Xue, B.; Guerin, S.; Li, H.; Zhang, L.; Liu, Y.; Shimon, L. J. W.; Si, M.; Cao, Y.; Wang, W.; Thompson, D.; Cai, K.; Yang, R.; Gazit, E. Co-Assembly Induced Solid-State Stacking Transformation in Amino Acid-Based Crystals with Enhanced Physical Properties. *Angew. Chem.* **2022**, *134*, e202201234.

(31) Wang, Z.; Cheng, Q.; Xing, P.; Cao, Z.; Hao, A. Hydrogen bonded co-assembly of aromatic amino acids and bipyridines that serves as a sacrificial template in superstructure formation. *Soft Matter* **2019**, *15*, 6596-6603.

(32) Xing, P.; Chen, H.; Xiang, H.; Zhao, Y. Selective Coassembly of Aromatic Amino Acids to Fabricate Hydrogels with Light Irradiation-Induced Emission for Fluorescent Imprint. *Adv. Mater*. **2018**, *30*, 1705633.

(33) Holeček, M. Histidine in Health and Disease: Metabolism, Physiological Importance, and Use as a Supplement. *Nutrients* **2020**, *12*, 3, 848.

(34) Burley, S. K.; Petsko, G. A. Amino-aromatic interactions in proteins. *FEBS Lett.* **1986**, *203*, 139-143.

(35) Steiner, T.; Koellner, G. Hydrogen bonds with π-acceptors in proteins: frequencies and role in stabilizing local 3D structures. *J. Mol. Biol.* **2001**, *305*, 535-557.

(36) Duan, G.; Smith, V. H.; Weaver, D. F. Characterization of Aromatic−Amide (Side-Chain) Interactions in Proteins through Systematic ab Initio Calculations and Data Mining Analyses. *J. Phys. Chem. A* **2000**, *104*, 4521-4532.

(37) Hughes, R. M.; Waters, M. L. Effects of Lysine Acetylation in a β-Hairpin Peptide: Comparison of an Amide−π and a Cation−π Interaction. *J. Am. Chem. Soc*. **2006**, *128*, 13586-13591.

(38) Toth, G.; Murphy, R. F.; Lovas, S. Investigation of Aromatic-Backbone Amide Interactions in the Model Peptide Acetyl-Phe-Gly-Gly-N-Methyl Amide Using Molecular Dynamics Simulations and Protein Database Search. *J. Am. Chem. Soc*. **2001**, *123*, 11782-11790.

(39) Levitt, M.; Perutz, M. F. Aromatic rings act as hydrogen bond acceptors. *J. Mol. Biol*. **1988**, *201*, 751-754.

(40) Perutz, M. F. The role of aromatic rings as hydrogen-bond acceptors in molecular recognition. *Trans. R. Soc. A* **1993**, *345*, 105-112.

(41) Meyer, E. A.; Castellano, R. K.; Diederich, F. Interactions with Aromatic Rings in Chemical and Biological Recognition. *Angew. Chem. Int. Ed*. **2003**, *42*, 1210-1250.

(42) Trachsel, M. A.; Ottiger, P.; Frey, H. M.; Pfaffen, C.; Bihlmeier, A.; Klopper, W.; Leutwyler, S. Modeling the Histidine–Phenylalanine Interaction: The NH···π Hydrogen Bond of Imidazole·Benzene. *J. Phys. Chem. B* **2015**, *119*, 7778-7790.

(43) Liu, Q.; Wan, K.; Shang, Y.; Wang, Z.-G.; Zhang, Y.; Dai, L.; Wang, C.; Wang, H.; Shi, X.; Liu, D.; Ding, B. Cofactor-free oxidase-mimetic nanomaterials from self-assembled histidine-rich peptides. *Nat. Mater*. **2021**, *20*, 395-402.

(44) Du, P.; Liu, S.; Sun, H.; Wu, H.; Wang, Z. G. Designed histidine-rich peptide self-assembly for accelerating oxidase-catalyzed reactions. *Nano Res*. **2022**, *15*, 5, 4032-4038.

(45) Arnon, Z. A.; Kreiser, T.; Yakimov, B.; Brown, N.; Aizen, R.; Shaham-Niv, S.; Makam, P.; Qaisrani, M. N.; Poli, E.; Ruggiero, A.; Slutsky, I.; Hassanali, A.; Shirshin, E.; Levy, D.; Gazit, E.

On-off transition and ultrafast decay of amino acid luminescence driven by modulation of supramolecular packing. *iScience* **2021**, *24*, 7, 102695.

(46) Datta, D.; Tiwari, O.; Ganesh, K. N. New archetypes in self-assembled Phe-Phe motif induced nanostructures from nucleoside conjugated-diphenylalanines. *Nanoscale* **2018**, *10*, 3212-3224.

(47) Tiwari, O. S.; Ganesh, K. N.; Gazit, E. Effect of Stereochemistry and Hydrophobicity on the Self-Assembly of Phe-Phe-Nucleoside Conjugates. *Macromol. Chem. Phys*. **2022**, *223*, 2200011.

(48) Adler-Abramovich, L.; Marco, P.; Arnon, Z. A.; Creasey, R. C. G.; Michaels, T. C. T.; Levin, A.; Scurr, D. J.; Roberts, C. J.; Knowles, T. P. J.; Tendler, S. J. B.; Gazit, E. Controlling the Physical Dimensions of Peptide Nanotubes by Supramolecular Polymer Coassembly. *ACS Nano* **2016**, *10*, 8, 7436-7442.

(49) Kraft, M. L.; Weber, P. K.; Longo, M. L.; Hutcheon, I. D.; Boxer, S. G. Phase Separation of Lipid Membranes Analyzed with High-Resolution Secondary Ion Mass Spectrometry. *Science* **2006**, *313*, 1948-1951.

(50) Ross, P. D.; Subramanian, S. Thermodynamics of Protein Association Reactions: Forces Contributing to Stability. *Biochemistry* **1981**, *20*, 3096-3102.

(51) Wang, S. H.; Liu, F. F.; Dong, X. Y.; Sun, Y. Thermodynamic Analysis of the Molecular Interactions between Amyloid β-Peptide 42 and (−)-Epigallocatechin-3-gallate. *J. Phys. Chem. B* **2010**, *114*, 11576-11583.

(52) Chakraborty, S.; Mukherjee, S. Role of Small Moiety of a Large Ligand: Tyrosine Templated Copper Nanoclusters. *J. Phys. Chem. Lett*. **2021**, *12*, 3266-3273.

Table of Contents

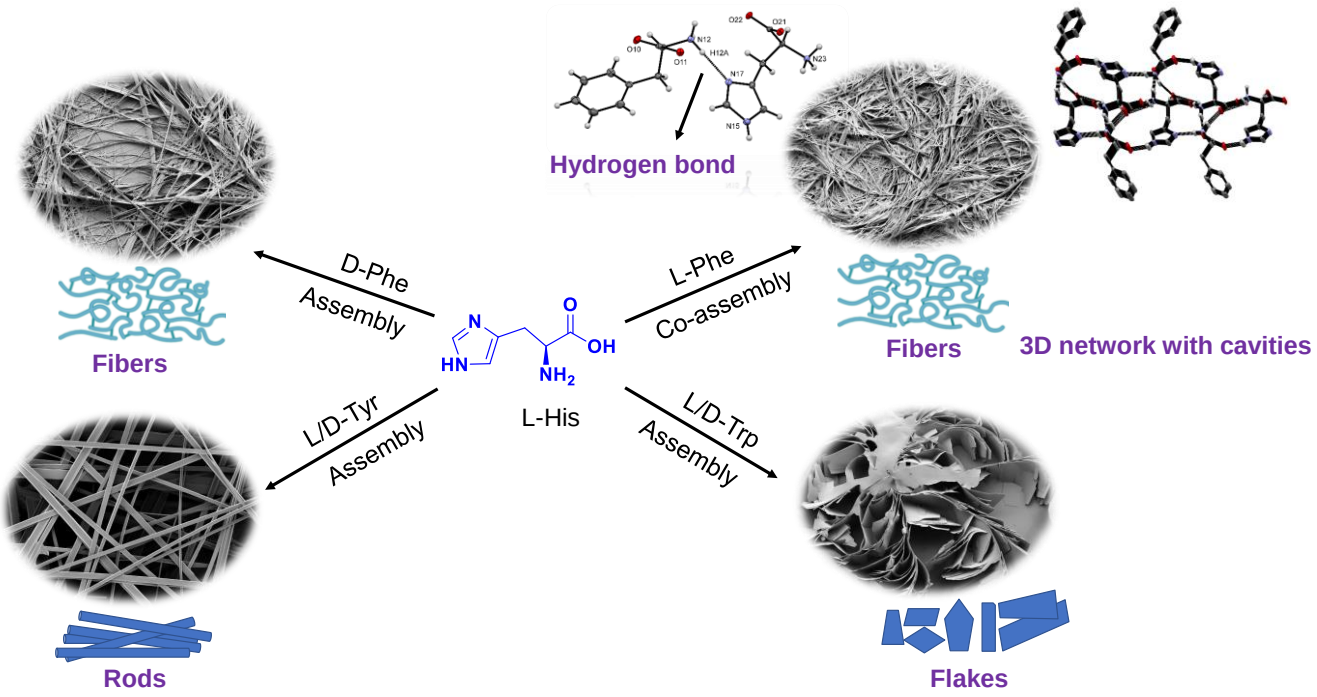

In this work, we explored the co-assembly of L-His with all aromatic amino acids, including Phenylalanine (Phe), Tyrosine (Tyr), and Tryptophan (Trp), all in both enantiomeric forms. By using the co-assembly approach, we expanded the field of amino acid based nano-materials and showed for the first time the ability to obtain discrete supramolecular nanostructures containing L-His based on its specific interactions with L-Phe.

Institute and/or researcher Twitter usernames: @TelAvivUni, @GazitLab and @AapkaTiwari